

Radio Emission from Cosmic Ray Air Showers based on Shower Simulations: On the Importance of a Realistic Atmospheric Index of Refraction

Klaus WERNER

SUBATECH, Université de Nantes – IN2P3/CNRS – EMN, Nantes, France

Krijn D. DE VRIES, Olaf SCHOLTEN

Kernfysisch Versneller Instituut, University of Groningen, 9747 AA, Groningen, The Netherlands

We present a macroscopic calculation of coherent electro-magnetic radiation from air showers initiated by ultra-high energy cosmic rays, based on currents obtained from three-dimensional Monte Carlo simulations of air showers in a realistic geo-magnetic field. We discuss the importance of a correct treatment of the index of refraction in air, given by the law of Gladstone and Dale, which affects the pulses enormously for certain configurations, compared to a simplified treatment using a constant index. We also provide some information about the numerical procedures referred to as EVA 1.0.

I. INTRODUCTION

The aim of our work is to provide a realistic calculation of radio emission from air showers, which might be used finally to analyze and understand the results from radio detection experiments (LOPES [1, 2], CODALEMA [3], LOFAR [4], and the new set-ups at the Pierre Auger Observatory (MAXIMA [5], AERA [6]).

There are two ways to compute the electric fields created by the moving charges of airshowers: the “macroscopic approach” adds up the elementary charges and currents to obtain a macroscopic description of the total electric current in space and time, which is the source of the electric field obtained from solving Maxwell’s equations. The “microscopic approach” computes the fields for each elementary charge, and adds then all the fields (with a large amount of cancellations).

Already in the earliest works of [7–10], a macroscopic treatment of the radio emission was proposed, but at the time the assumptions about the currents were rather crude. There is recent progress concerning the macroscopic approach. In 2007, we performed calculations allowing under simplifying conditions to obtain a simple analytic expression for the pulse shape, showing a clear relation between the pulse shape and the shower profile [11]. This allows, for example, to determine from the radio signal the chemical composition [12] of the cosmic ray. The picture used was very similar to the one in Ref. [8], which has been refined by using a more realistic shower profile and where we calculate the time-dependence of the pulse. Recently it was confirmed that the pulse predicted in the microscopic description [13, 14] agrees with the predictions following from the macroscopic picture as shown in [15].

In Ref. [16], we advance further by computing first the four-current from a realistic Monte Carlo simulation (in the presence of a geo-magnetic field), and then solve the Maxwell equations to obtain the electric field, while con-

sidering a realistic (variable) index of refraction, given by the Gladstone-Dale law as

$$n = n_{GD} = 1 + 0.226 \frac{\text{cm}^3}{g} \rho(h), \quad (1)$$

with $\rho(h)$ being the density of air at an atmospheric height h . Although this index varies only between 1 and 1.0003, this variation has important consequences, as discussed in detail in Ref. [16]. For example, the retarded time t^* (the time when the signal was sent out) for a given observer position is a multivalued function of the observer time t , which gives rise to “Cherenkov effect” phenomena, where the signal may become very short and very strong. The caveat in this treatment is the fact that we consider the currents to be point-like, which is only a good approximation far from the shower axis. The Cherenkov-like effects actually show up as singularities, and we expect these singularities to disappear when we give up the “point-like” assumption. Nevertheless, although Ref. [16] does not provide a realistic picture for all observer distances, its results are very important as the basis of the much more realistic description employed in the present paper.

Anyhow, the notion “point-like” has to be taken with care. In the point-like picture described in Ref. [16], we do not have a simple moving point-like charge, we rather have already transverse currents, and also the longitudinal structure is nontrivial, just all these currents are – at a given time – concentrated in a very small volume. But there must be an internal structure, and therefore it is natural as a next step to investigate the three-dimensional structure of the shower at a given time. In order to do so, we consider a “shower fixed” coordinate system. The origin O of this system is the center of the shower front. We use the coordinates x and y to describe positions on the plane transverse to the shower axis, and h as the longitudinal distance behind the shower front. The latter one is actually a hypothetical plane, which contains real

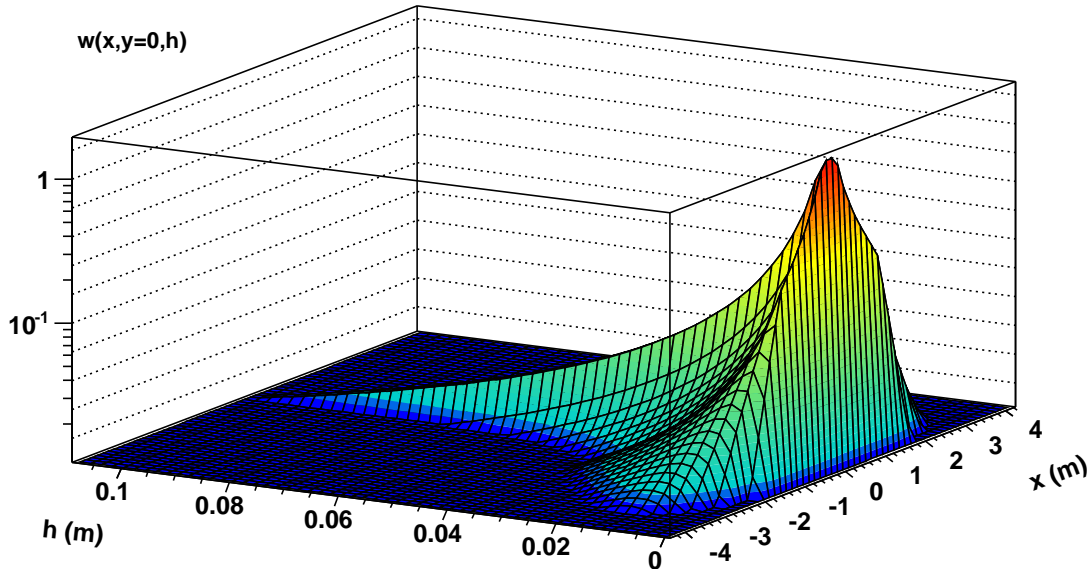


Figure 1: The distribution of charged particles $w(x, y, h)$ at a given time, as a function of the transverse coordinate x and the longitudinal coordinate h , for $y = 0$.

particles only around $x = y = 0$, whereas for larger distances, the fastest particles stay behind this plane. The situation as obtained in a realistic Monte Carlo simulation (details to be discussed later) is shown in fig. 1. The distribution of charged particles shows a very sharp maximum at the origin ($x = y = h = 0$), and falls steeply in transverse and longitudinal direction. We will discuss the functional form of this distribution later in detail, for the moment we only want to illustrate the fact that the distribution obtained from simulations shows nontrivial structures, concentrated in a small range in particular concerning the h variable.

In the current paper, we want to take into account the realistic three-dimensional form (at a given time) of the shower, as obtained from shower simulations, still using a realistic index of refraction. The numerical procedures of our approach, referred to as EVA 1 (Electric fields, using a Variable index of refraction in Air shower simulations), amount to air shower simulations, analysis tools for extracting currents and shower shapes, and automatic fitting procedures providing smooth functions for all relevant shower characteristics. First results of our new approach have been published recently [17].

II. TAMING SINGULARITIES

We first repeat some elementary facts of the shower evolution, which have been discussed in detail in Ref. [16].

We consider here showers due to a very energetic primary particle, with an energy above 10^{14} eV. Such a shower moves with a velocity βc , which is very close to the vacuum velocity of light c . There is a constant creation of electrons and positrons at the shower front, with somewhat more electrons than positrons (electron excess). This is compensated by positive ions in the air, essentially at rest. The electrons and positrons of the shower scatter and lose energy, and therefore they move slower than the shower front, falling behind, and finally drop out as “slow electrons / positrons”. Close to the shower maximum, the charge excess of the “dropping out” particles is compensated by the positive ions, since there is no current before or behind the shower. Taking all together we have the situation of a moving charge, moving with the vacuum velocity of light, even though the electrons and positrons are moving slower, and they are deviated (in opposite directions) in the Earth magnetic field.

Neglecting the finite dimension of the shower, referred to as “point-like” (PL) approximation, one has a four-current

$$j_{\text{PL}}(t', \vec{x}) = J(t') \delta^3(\vec{x} - \vec{\xi}(t')), \quad (2)$$

with a longitudinal component due to charge excess, and a transverse component due to the geo-magnetic field. Solving Maxwell’s equations, we can express the potential in terms of the four-current J , evaluated at the retarded

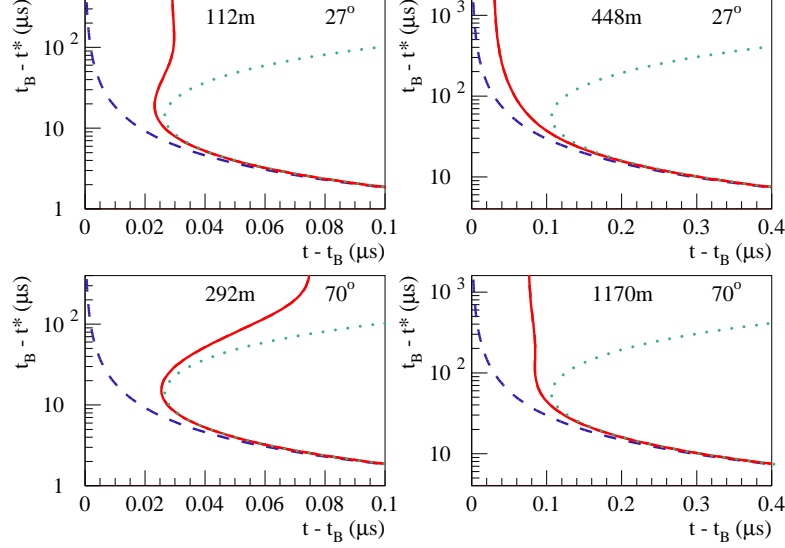


Figure 2: The dependence of the retarded time t^* on the observer time t for $n = 1$ (dashed line), $n = n_{GD}$ (solid line), and $n = n_{\text{ground}} \approx 1.0003$ (dotted line) for inclined showers (27° and 70° and for different distances in meters of the observer from the impact). The reference time t_B is the time of closest approach of the shower with respect to the observer.

time t^* , as [16]

$$A_{\text{PL}}^\beta(t, \vec{x}) = \frac{\mu_0}{4\pi} \frac{J^\beta}{|\tilde{R}V|}, \quad (3)$$

with $V = c^{-1}d\xi/dt'$, and with \tilde{R} being a four-vector defined as $\tilde{R}^0 = c(t - t^*)$ and $\tilde{R}^i = -L\partial/\partial\xi^i L$, where L is the optical path length between the source $\vec{\xi}(t^*)$ and the observer. This point-like approximation is certainly only valid at large impact parameters (> 500 m), but even more importantly it will serve as a basis for more realistic calculations, as discussed later. It should be noted that in case of $n > 1$ and even more for $n = n_{GD}$ the vector potential shows singularities, which arise from $1/|\tilde{R}V| \propto dt^*/dt$ and the fact that t^* is a non-monotonic function of t , as shown in fig. 2 and discussed in detail in [16]. We show the realistic case $n = n_{GD}$ with the corresponding curve situated between the two limiting cases $n = 1$ and $n = 1.0003$.

In general, one needs to consider the finite extension of the shower at a given time t' , expressed via a weight function $w(r^1, r^2, h)$, where r^1 and r^2 represent the transverse distance from the shower axis, and h the longitudinal distance from the shower front, the latter one moving by definition with the vacuum velocity of light. Positive h means a position behind the shower front, and therefore w is non-vanishing only for positive h . The weight will fall off rapidly with increasing distance $r = \sqrt{(r^1)^2 + (r^2)^2}$ from the axis. The precise form of w will be discussed in

a later chapter. In principle one needs to convolute the weight w with the currents, and then compute the potential and field. Due to a translation invariance (being correct to a very good approximation, since the index of refraction varies slowly), this is the same as computing first the potential in PL approximation, and then performing a convolution as

$$A^\beta(t, \vec{x}) = \int d^2r \int dh w(\vec{r}, h) A_{\text{PL}}^\beta(t, x^\parallel - h, \vec{x}_\perp + \vec{r}). \quad (4)$$

where x^\parallel and $\vec{x}_\perp = (x^{\perp 1}, x^{\perp 2})$ are coordinates parallel and transverse to the shower axis. Defining $\vec{y}^\perp = \vec{x}_\perp + \vec{r}$, we get

$$A^\beta(t, \vec{x}) = \int d^2y^\perp \int dh w(\vec{y}^\perp - \vec{x}_\perp, h) A_{\text{PL}}^\beta(t, x^\parallel - h, \vec{y}^\perp). \quad (5)$$

The electric field is then obtained from the derivatives of A .

One cannot simply exchange derivation and integration, due to the presence of singularities as discussed before, and therefore a naive convolution of w with \vec{E}_{PL} is not possible: one needs a more sophisticated treatment of the singularities. So let us consider the most general case of a multi-valued function t^* as a function of the observation time t , as sketched in fig. 3. The function is composed of several branches, br_n , limited by certain times t_k . The derivative dt^*/dt becomes infinite at these branch endpoints, and the point-like potential becomes

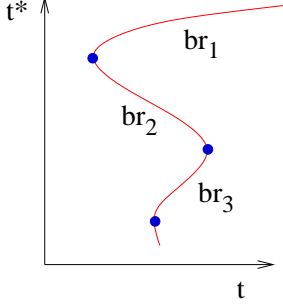


Figure 3: Several branches of the function of t^* versus t , where t^* is the retarded time corresponding to an observer time t .

singular. This is why we refer to the t_k as "critical times". Close to these singularities, we have

$$t^* - t^*(t_k) \sim |t - t_k|^{1/2}, \quad \text{and} \quad \frac{dt^*}{dt} \sim |t - t_k|^{-1/2}. \quad (6)$$

When evaluating eq. (5), we have to worry about the critical time for a given observer position $(x^\parallel - h, \vec{y}^\perp)$, corresponding to the arguments of A_{PL} . In other words, t_k is a function of these variables, i.e.

$$t_k = t_k(x^\parallel - h, \vec{y}^\perp). \quad (7)$$

It is useful to define a "critical h value" h_k , for given t , via

$$t = t_k(x^\parallel - h_k, \vec{y}^\perp), \quad (8)$$

which allows us to write eq. (5) for a single branch as

$$A^\beta(t, \vec{x}) = \int d^2 y^\perp \int_0^{h_k} dh w(\vec{y}^\perp - \vec{x}^\perp, h) A_{\text{PL}}^\beta(t, x^\parallel - h, \vec{y}^\perp). \quad (9)$$

Using the integration variable $\lambda = h_k - h$, we obtain our master formula for the vector potential,

$$A^\beta(t, \vec{x}) = \int d^2 y^\perp \int_0^{h_k} d\lambda w(\vec{y}^\perp - \vec{x}^\perp, h_k - \lambda) A_{\text{PL}}^\beta(t, x^\parallel - h_k + \lambda, \vec{y}^\perp), \quad (10)$$

which is useful because A_{PL} has a singularity in λ for $\lambda \rightarrow 0$, which does not interfere with the derivatives which have to be performed in order to get the fields. In the following we keep in mind that A_{PL}^β has the following arguments: the time t , the longitudinal variable $x^\parallel - h_k + \lambda$, and the transverse variable \vec{y}^\perp ; w has the arguments $h_k - \lambda$ and $\vec{y}^\perp - \vec{x}^\perp$. We do not write these arguments explicitly, to simplify the notation. We also omit the arguments t, \vec{x} of the vector potential. So we write

$$A^\beta = \int d^2 y^\perp \int_0^{h_k} d\lambda w A_{\text{PL}}^\beta. \quad (11)$$

The components of the electric field are

$$E^\parallel = c \left(-\frac{\partial A^0}{\partial x^\parallel} - \frac{\partial A^\parallel}{\partial ct} \right) \quad (12)$$

$$E^{\perp i} = c \left(-\frac{\partial A^0}{\partial x^{\perp i}} - \frac{\partial A^{\perp i}}{\partial ct} \right). \quad (13)$$

Using $A_{\text{PL}}^i = \frac{\mu_0}{4\pi} J^i |\tilde{R}V|^{-1}$ and eqs. (A1,A2), the time derivative of the vector potential may be written as

$$\frac{\partial A^i}{\partial ct} = \int d^2 y_\perp \int_0^{h_k} d\lambda \left\{ -w' A_{\text{PL}}^i + w \dot{A}_{\text{PL}}^i \right\}, \quad (14)$$

with $w' = \partial w / \partial h$, $\dot{A}_{\text{PL}}^i = \frac{\mu_0}{4\pi} K^i |\tilde{R}V|^{-1}$, $K = dJ/dt'$. In principle there is an additional term from the time derivative of the upper limit of integration, but this contribution vanishes due to $w(0) = 0$ (see next chapter). Concerning the space derivative, we first compute the derivative with respect to the longitudinal variable. We find

$$-\frac{\partial}{\partial x^\parallel} A^0 = - \int d^2 y_\perp \int_0^{h_k} w' A_{\text{PL}}^0 d\lambda \quad (15)$$

since the total longitudinal space derivative of A_{PL}^0 vanishes exactly. The transverse derivatives of the scalar potential can be expressed in terms of the derivatives $w^i = \partial w / \partial r^i$ of the weight function w as

$$-\frac{\partial}{\partial x^{\perp i}} A^0 = \int d^2 y_\perp \int_0^{h_k} d\lambda w^i A_{\text{PL}}^0. \quad (16)$$

The above results for the partial derivatives of the vector potential A^μ allow us to obtain corresponding expressions for the electric field. The longitudinal electric field $c(\partial^\parallel A^0 - \partial^0 A^\parallel)$ is given as

$$E^\parallel = -c \int d^2 y_\perp \int_0^{h_k} d\lambda \left\{ w' A_{\text{PL}}^0 - w' A_{\text{PL}}^\parallel + w \dot{A}_{\text{PL}}^\parallel \right\}. \quad (17)$$

The transverse field $c(\partial^{\perp i} A^0 - \partial^0 A^{\perp i})$ can be written as

$$E^{\perp i} = c \int d^2 y_\perp \int_0^{h_k} d\lambda \left\{ w^i A_{\text{PL}}^0 + w' A_{\text{PL}}^{\perp i} - w \dot{A}_{\text{PL}}^{\perp i} \right\}. \quad (18)$$

The formulas simplify considerably, far from the singularity as well as at the singularity, but we keep the exact expressions, in order to interpolate correctly between the two extremes. It should be noted that the above expression concern a single branch, the complete field is the sum over all branches.

III. MONTE CARLO SIMULATIONS AND FITTING PROCEDURES: EVA 1.0

The numerical evaluation of the eqs. (17,18) is done employing the EVA 1.0 package, which

- provides the weights w ,
- provides the currents J needed to compute the potentials A_{PL}^μ ,
- does the numerical integration of eqs. (17,18) and the summation over branches.

Both the weights w and the point-like currents J are obtained from realistic Monte Carlo simulations of air showers. The EVA package consists of several elements:

- the airshower simulation code CX-MC-GEO, including analysis tools to extract four-currents and the shape of the shower,
- the automatic fitting procedure FITMC which allows to obtain analytical expressions for the currents,
- the EVA program which solves the non-trivial problem to compute the retarded time and “the denominator” $\tilde{R}V$, for a realistic index of refraction.

We first discuss airshowers. They are considered point-like for the moment, as seen by a far-away observer. The shower is a moving point, defining a straight line trajectory, see fig. 4. One defines an “observer level” which is a

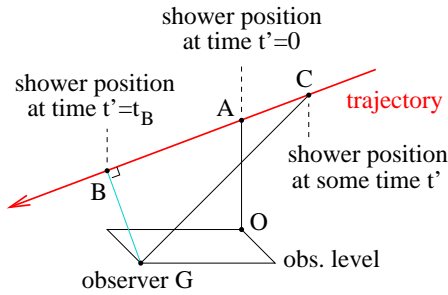


Figure 4: Air shower as seen by an observer G . The point B is the point of closest approach with respect to the observer G . The point C is the shower position at some time t' . The point B corresponds to the shower position at $t' = t_B$ (which may be taken to be zero).

plane of given altitude z with respect to the sea level. One defines some arbitrary point A on the trajectory. The corresponding projection to the observer level is named O (origin) and the observer position is given in terms of coordinates (x, y) with respect to O . The x -axis is the intersection of the “shower plane” OAC and the observer level. The angle between the shower trajectory and the vertical axis OA is referred to as inclination and denoted as θ . In many applications, A and O coincide: in this case they represent the impact point. For horizontal showers the two points are different. The geomagnetic field is specified by an angle α with respect to the vertical, and an angle ψ with respect to the shower plane

($\psi = 0$ means that \vec{B} points towards the shower origin). One can of course see it the other way round (maybe even more natural): for a given orientation of the geomagnetic field, ψ defines the orientation of the shower axis.

In the EVA framework, one has to specify the altitude z , the distance $a = |OA|$, the inclination θ , the energy E of the shower, and the observer coordinates x, y . And in addition the angles α and ψ and the magnitude B of the geomagnetic field.

The actual airshower simulations are done with a simulation program called CX-MC-GEO, being part of the EVA package. It is based on CONEX [18, 19], which has been developed to do air shower calculations based on a hybrid technique, which combines Monte Carlo simulations and numerical solutions of cascade equations. It is also possible to run CONEX in a pure cascade mode, and this is precisely what we use. This provides full Monte Carlo airshower simulations, using EGS4 for the electromagnetic cascade, and the usual hadronic interaction models (QGSJET, EPOS, etc) to simulate hadronic interactions.

Two features have been added to CONEX. First of all a magnetic field, which amounts to replacing the straight line trajectories of charged particles by curved ones. This concerns both the electromagnetic cascade and the hadronic one. In addition, analysis tools have been developed, which allow to get a complete information of charged particle flow in space and time. These features have already been developed to compute currents in [16], so in particular more details about the implementation of the magnetic field can be found there (though we did not use the names EVA and CX-MC-GEO yet). We also discuss in [16] some details about the different internal coordinate systems needed to extract information about currents. The results shown in [17] were also based on CX-MC-GEO simulations, referred to as CONEX-MC-GEO at the time.

In [16], we provide several results concerning particle numbers and currents for different orientations of the axis with respect to the geomagnetic field. All the results are still valid, the corresponding programs did not change since.

An important ingredient of our approach is the parametrization of the results (currents J , distributions w), which have been obtained from simulations in the form of discrete tables. This is necessary partly to perform semi-analytical calculations such that numerically stable functions have to be dealt with without having huge cancellations in the results. It is especially important for the stable calculation of Cherenkov effects. It allows for the calculation of a smooth shower evolution, whereas when working with histogrammed distributions in position and time, it is not possible to reconstruct a continuous shower evolution and the artificially introduced sudden changes in the particle trajectories may give rise to spurious radio

signals.

The parametrization of Monte Carlo distributions is done in FITMC. This program takes the distributions (for currents) as obtained from the simulations in the form of histograms, to obtain analytical expressions, using standard minimization procedures. FITMC creates actually computer code to represent the analytical functions, and this code is then executed at a later stage. The “basic distribution” is the so-called “electron number N ” (which counts the number of electrons and positrons) as a function of the shower time t' , which is fitted as

$$N(t') = A \exp(B + C(t' + D) + E(t' + F)^2 + G(t' + H)^3) \quad (19)$$

As an illustration, we show here the case of a shower with an initial energy of $5 \cdot 10^{17}$ eV, an inclination $\theta = 27^\circ$, and an azimuth angle $\psi = 0^\circ$, defined with respect to the magnetic north pole. The angle ψ refers to the origin of the shower. So $\psi = 0^\circ$ thus implies that the shower moves from north to south. We consider the magnetic field at the CODALEMA site, i.e. $|\vec{B}| = 47.3 \mu T$ and $\alpha = 153^\circ$, so the shower makes an angle of roughly 54° with the magnetic field. In fig.5, we plot the electron number N ,

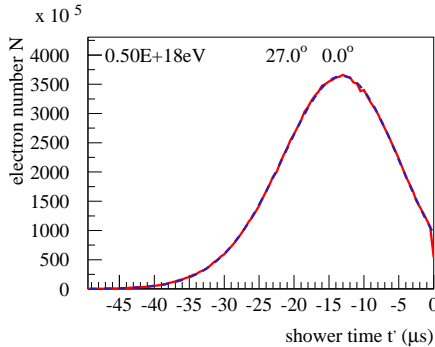


Figure 5: The number N of electrons and positrons, as a function of the shower time t' for a shower with an inclination $\theta = 27^\circ$ and an azimuth angle $\psi = 0^\circ$ with respect to the magnetic north pole. The full red line represents the simulation result, the dashed blue line is the fit.

as a function of the shower time t' , for a simulated single event, together with the fit curve. A thinning procedure has been applied (here and in the following) to obtain the shown simulation results. The time $t' = 0$ refers to the point of closest approach with respect to an observer at $x = 0$, $y = 500$ m, $z = 140$ m. We suppose $a = 0$ (so the shower hits the ground at $x = y = 0$).

The magnitudes of the components J^μ of the currents have a similar t' dependence as $N(t')$. Therefore we parametrize the ratios $J^\mu/(Nec)$, with N being the electron number, e the elementary charge, and c the velocity

of light. We use the following parametric form:

$$\frac{J^\mu(t')}{N(t')ec} = A + B(x + C) + D(x + E)^2 + F(x + G)^3. \quad (20)$$

In fig. 6, we plot the longitudinal current component J^z

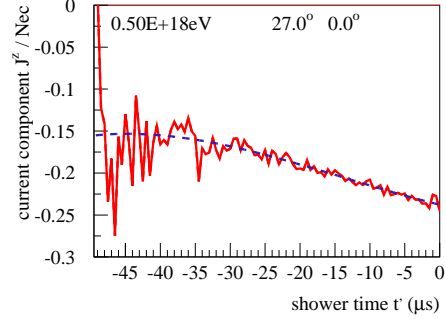


Figure 6: The longitudinal current component J^z , divided by Nec , as a function of the shower time t' . The full red line represents the simulation result, the dashed blue line is the fit.

(divided by Nec), as a function of the shower time t' , for a simulated single event, together with the fit curve. At early times - far away from the shower maximum - there are of course large statistical fluctuations. But since $N(t')$ is very small here, this region does not contribute to the pulse. In fig. 7, we plot the transverse current

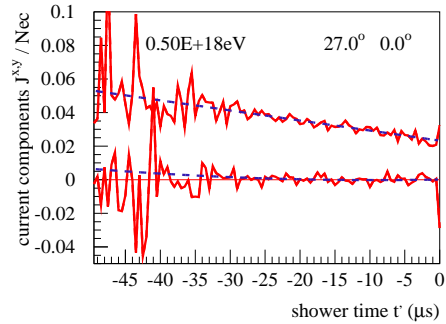


Figure 7: The transverse current components J^x (lower lines) and J^y (upper lines), divided by Nec , as a function of the shower time t' . The full red lines represents the simulation result, the dashed blue lines are the fits.

components J^x and J^y , (divided by Nec), as a function of the shower time t' , for a simulated single event, together with the fit curves.

The EVA program uses these analytical fit functions for the current components,

$$J^\mu = \left\{ \frac{J^\mu}{Nec} \right\}_{fit} \cdot N_{fit} \cdot e \cdot c, \quad (21)$$

to compute the vector potential. The currents have to be evaluated at $t' = t^*$, the retarded time. The central part of EVA is actually the determination of the retarded time $t^*(t, \vec{x})$ for a given observer position. This is quite involved – in case of a realistic index of refraction – and described in detail in [16] (again without referring to EVA, but these are exactly the same programs being used). A results of such a calculation is shown in fig. 2.

A new feature compared to [16] – and most relevant for this paper – is the possibility to obtain information about the shape of the shower via the weight function w . The weight function w is not perfectly cylindrically symmetric, due to the geo-magnetic field but also due to statistical fluctuations, since we are considering individual Monte Carlo events. However, in this paper we will neglect these tiny deviation from symmetry, and consider a weight function $w(r, h)$ depending only on the two variables r and h , related to the general weight function as

$$w(r, h) = 2\pi r w(\vec{r}, h). \quad (22)$$

The lateral coordinate r measures the transverse distance from the shower axis, the longitudinal coordinate h is meant to be the distance behind the shower front. This front is a hypothetical point moving along the shower axis with the velocity of light c , such that all the particles are behind this front, expressed by a positive value of h . We will express the weight function as

$$w(r, h) = w_1(r) w_2(r, h), \quad (23)$$

with $\int dr w_1(h) = 1$, and with $\int dh w_2(r, h) = 1$ for all values of r .

We use again CX-MC-GEO to obtain w , then FITMC to obtain an analytical function, which is later used in the EVA program to compute the fields, based on the formulas described in the preceding chapter. All the simulation results shown in the following are based on the the same shower, mentioned earlier when discussing currents.

We first investigate the radial distribution $w_1(r)$. In fig. 8, we show the radial distribution as obtained from the Monte Carlo simulation. The thin lines correspond to different times t' , between $-25 \mu s$ and $-5 \mu s$. The points represent an average over all times, and also averaged over r -bins. Since the time dependence is quite small, we will use the radial distribution at the shower maximum t'_{\max} as time-independent distribution $w_1(r)$. The thick red line corresponds to a fit to the Monte Carlo data, using the form

$$w_1(r) = \frac{\Gamma(4.5 - s)}{\Gamma(s)\Gamma(4.5 - 2s)} \left(\frac{r}{r_0}\right)^{s-1} \left(\frac{r}{r_0} + 1\right)^{s-4.5}, \quad (24)$$

with fit parameters r_0 and s (providing an excellent fit).

Knowing $w_1(r)$, we now investigate how far the particles are moving behind the shower front, expressed in

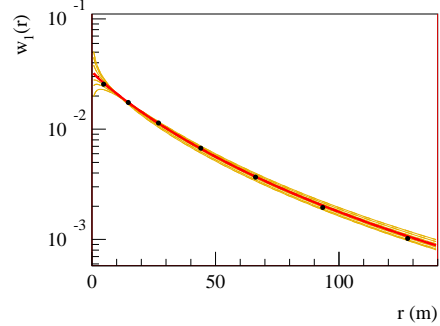


Figure 8: The radial distribution $w_1(r)$. The thin yellow lines correspond to different times, the points represent an average, and the thick red line corresponds to a fit (see text).

terms of the longitudinal distance h , for a given transverse distance r . From the above simulation, we obtain easily the mean distance \bar{h} at a given r . We find a perfectly linear time dependence, of the form

$$\bar{h} = h_0 + c\Delta\beta t', \quad (25)$$

where $\Delta\beta$ can be obtained from fitting time dependence at different distances r , the result is shown in fig. 9 as solid line. The quantity $\Delta\beta$ represents the veloc-

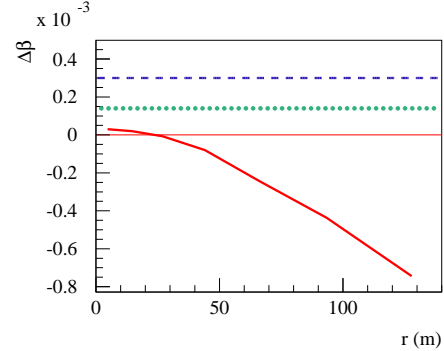


Figure 9: The longitudinal velocity difference $\Delta\beta$ versus r . We show the results for realistic simulations (thick red solid line) and for $\gamma = 60$ (green dotted line). Also shown: the value $1 - 1/n_{\text{ground}}$ (blue dashed line).

ity difference (in units of c) with respect to the the shower front, which itself moves with velocity c . So the velocity of the “average position” of the shower is $1 - \Delta\beta$. Also shown in fig. 9, as dashed line, is the value $1 - 1/n_{\text{ground}}$, corresponding to the velocity of light in air with $n_{\text{ground}} = 1.0003$. And we also plot as dotted line the $\Delta\beta$ obtained from $\gamma = 60$, corresponding to the average electron energy. The simulated curve (thick full line) is considerably below this dashed and the dotted curves, which means that the velocity of the average positions is larger than c/n_{ground} , it is also larger than the

velocity of the average electron. The simulated velocity is even (slightly) larger than c . This is due to the fact that matter is moving on the average from inside (small r) to outside (large r), and the average \bar{h} decreases with decreasing distance r . But the effect is small, the deviation of the shower velocity from c is less than $1/1000$. We

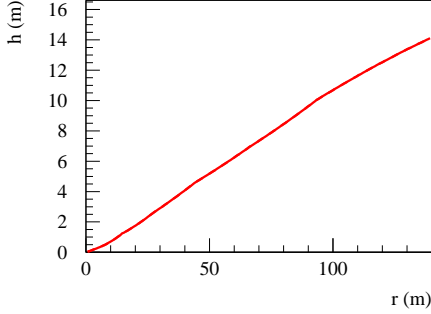


Figure 10: The mean value \bar{h} for given values of the lateral distance r .

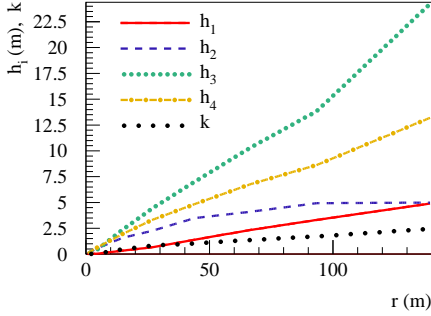


Figure 11: The parameters h_1 , h_2 , h_3 , h_4 , and k as a function of the lateral distance: h_1 (full line), h_2 (dashed line), h_3 (dotted line), h_4 (dashed-dotted line), k (wide-dotted line),

will ignore the small time dependence for the moment, and consider in the following quantities at t_{\max} . To get some idea about the typical scales of the h -distribution $w_2(r, h)$, for a given value of r , we determine the mean value \bar{h} , as shown in fig. 10. The mean value \bar{h} is almost a linear function of the distance r , and for $r = 100$ m we get an average h of roughly 10 m.

The w_2 distribution is obtained by fitting Monte Carlo data in a range h between zero and $5\bar{h}$, for given r . We use

$$w_2(r, h) = \begin{cases} w_2^{\text{MGD}}(r, h) & \text{for } r > r_0 \\ w_2^{\text{IGD}}(r, h) & \text{for } r \leq r_0 \end{cases}, \quad (26)$$

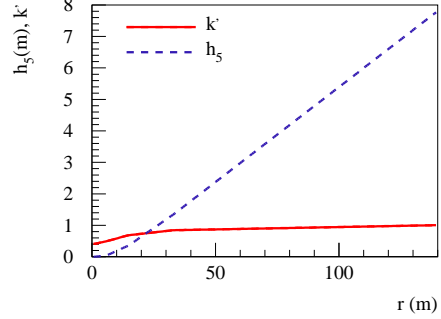


Figure 12: The parameters h_5 and k' as a function of the lateral distance: k' (full line), h_5 (dashed line)

with w_2^{MGD} being a “modified gamma distribution” of the form

$$w_2^{\text{MGD}}(r, h) = \frac{H(r, h) G(r, h)}{N(r)}, \quad (27)$$

with

$$H(r, h) = \Theta(h_1 - h) \left(2 \left(\frac{h}{h_1} \right) - \left(\frac{h}{h_1} \right)^2 \right) + \Theta(h - h_1), \quad (28)$$

and

$$G(r, h) = \Theta(h_3 - h) \left(h^{k-1} e^{-h/h_2} \right), \quad (29)$$

$$+ \Theta(h - h_3) \left(h_3^{k-1} e^{-h_3/h_2} e^{-(h-h_3)/h_4} \right),$$

with N being a normalization constant such that $\int dh w_2(r, h) = 1$. The function w_2^{IGD} is an “inverse gamma distribution” of the form

$$w_2^{\text{IGD}}(r, h) = \frac{(h_5)^{k'}}{\Gamma(k')} h^{-k'-1} e^{-h_5/h}.$$

We use $r_0 = 20$ m. The r -dependence is hidden in the parameters h_1 , h_2 , h_3 , h_4 , h_5 , k , and k' . In figs. 11 and 12, we plot the parameters, as obtained from fitting the Monte Carlo data. All parameters grow with increasing distance r . Whereas h_2 seems to saturate, all the other parameters grow roughly linearly with r . With these parameters, we get good fits for h values up to five times the mean. In figs. 13 and 14, we show the fits of w_2 together with Monte Carlo simulation results for different times. In fig. 15, we show the fitted w_2 curves for three different values of r , conveniently plotted as $\bar{h} w_2$ versus h/\bar{h} , where one clearly sees the evolution of the shape with r .

The reason to switch between w_2^{MGD} and w_2^{IGD} at $r_0 = 20$ m becomes clear from figures 13 through 15. From figure 15 it can be seen clearly that the particle

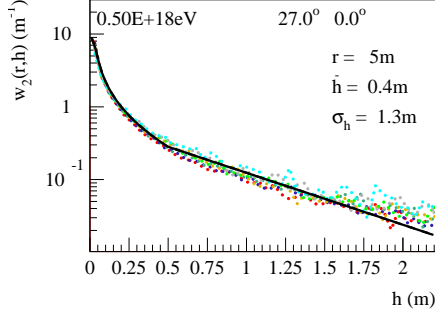


Figure 13: The distribution $w_2(r, h)$ for $r = 5$ m. The full black line represents the fit, the dotted lines are simulation results for different times.

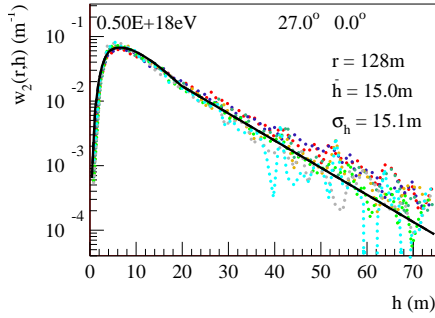


Figure 14: The distribution $w_2(r, h)$ for $r = 128$ m. The full black line represents the fit, the dotted lines are simulation results for different times.

distribution as obtained from the Monte-Carlo simulations behaves quite differently close to the shower axis as

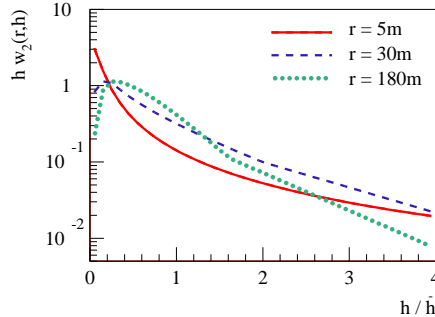


Figure 15: The distribution $w_2(r, h)$ for $r = 5$ m (full line), $r = 30$ m (dashed line), and $r = 180$ m (dotted line).

compared to the distribution at large distances. This different behavior requires the use of different fit-functions in both regimes. At large distances from the core, the parametrization of w_2^{MGD} reproduces the MC result accurately. At small distances, it is important to have a smooth parametrization without jumps in the first derivatives, which is the case when using w_2^{IGD} .

The above fit function w_2^{IGD} leads to a delta-peak at $r = 0$. To still obtain numerical stability, a cut-off for the values k' and h_5 is introduced such that the width of w_2^{IGD} is 1 mm. Since most of the particles are located at $r = \delta x^\perp = 1$ m from the shower axis, the path difference between signals emitted at this distance on both sides of the shower axis acts as the important length scale in this regime. We estimate this path difference δR for a constant index of refraction equal to $n = 1.0003$: we have $\delta R \approx \frac{\partial R}{\partial x^\perp} \delta x^\perp \approx \sqrt{n^2 \beta^2 - 1} \delta x^\perp \approx 3$ cm. Here we use that at the Cherenkov time (critical time for $h = 0$), we have $R^0 = n \beta x^\parallel$, and $x_c^\parallel = \sqrt{n^2 \beta^2 - 1} x_c^\perp$ [20]. So a cut-off of $w_2^{\text{IGD}} \approx 1$ mm should give stable results. This has been tested numerically.

IV. RESULTS

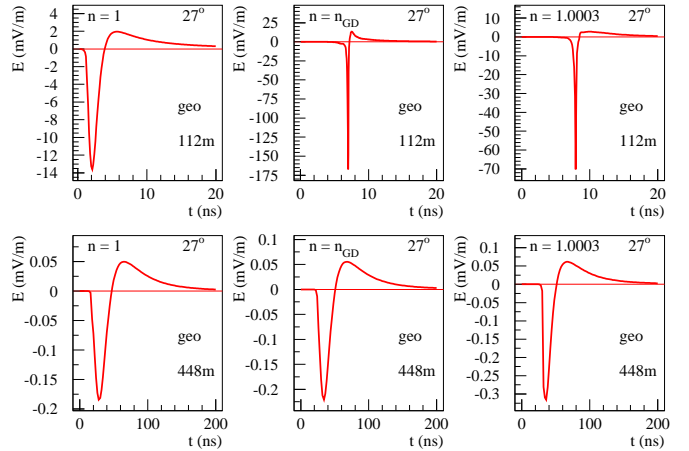


Figure 16: The y component of the geomagnetic contribution to the electric field as a function of the observer time t in ns, for an observer distance of 112 m (upper panel) and 448 m (lower panel). We compare different options for the index of refraction n , namely $n = 1$ (left), $n = n_{\text{GD}}$ (middle), and $n = 1.0003$ (right).

As already said, the eqs. (17,18) are evaluated employing the EVA 1.0 package, which provides the weights w , the currents J , the denominators $\tilde{R}V$, and the integration procedures, as discussed in the previous chapter.

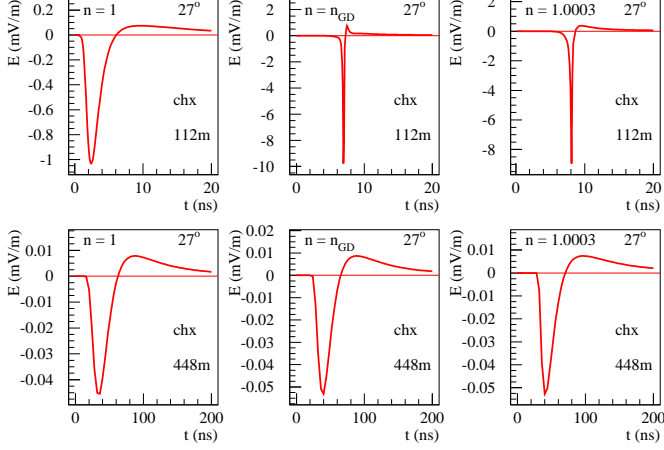


Figure 17: The x component of the charge excess contribution to the electric field as a function of the observer time t in ns, for an observer distance of 112 m (upper panel) and 448 m (lower panel). We compare different options for the index of refraction n , namely $n = 1$ (left), $n = n_{\text{GD}}$ (middle), and $n = 1.0003$ (right).

We first consider the same “reference shower” (inclination 27°) already discussed there. We will distinguish between the geomagnetic contribution (caused by the currents due to the geomagnetic field) and the contributions due to charge excess. In figs. 16 and 17, we show the results for the two contributions, for two different observer positions. We compare the realistic scenario ($n = n_{\text{GD}}$) with the two “limiting cases” $n = 1$ and $n = 1.0003$. One can clearly see big differences between the three scenarios, up to a factor of ten in width and magnitude. We also see, even in the realistic case ($n = n_{\text{GD}}$), the appearance of “Cherenkov-like” behavior, with very sharp peaks. In figs. 18 and 19, we consider a more inclined shower (70°). The differences between the realistic case ($n = n_{\text{GD}}$) and the two “limiting cases” is even bigger: more than a factor of 100 in width and magnitude! In fig. 20, the Fourier spectrum is shown for the geomagnetic component of the electromagnetic field for a 70 degrees inclined shower and an observer positioned at $d = 1170$ m from the impact point of the shower corresponding to an impact parameter b of around 400 m. At this distance the shower maximum occurs at the Cherenkov height ($b/\tan \alpha_{\text{Cherenkov}}$) for a realistic index of refraction. The realistic case ($n = n_{\text{GD}}$) contains very high frequency components up to several GHz as one would expect from the sharp peak in figure 18. The two limiting cases peak at lower frequencies below 100 MHz. This “Cherenkov-like” behavior for the realistic case might have been observed by the ANITA-collaboration [21], where pulses have been measured in the 200-1200 MHz band. Furthermore, since these high

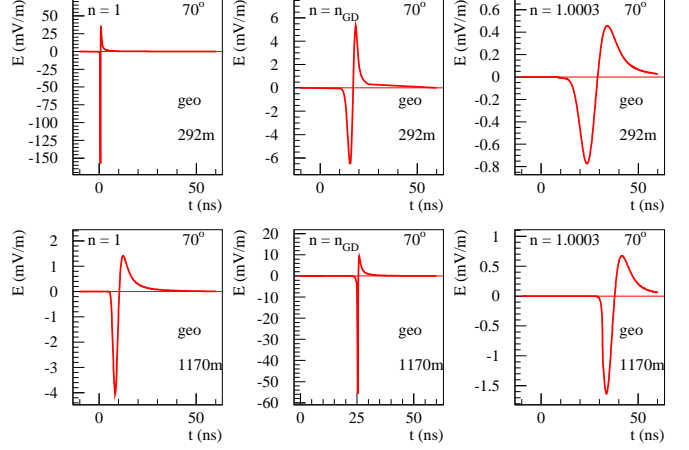


Figure 18: Same as fig 16, but here we consider a more inclined shower.

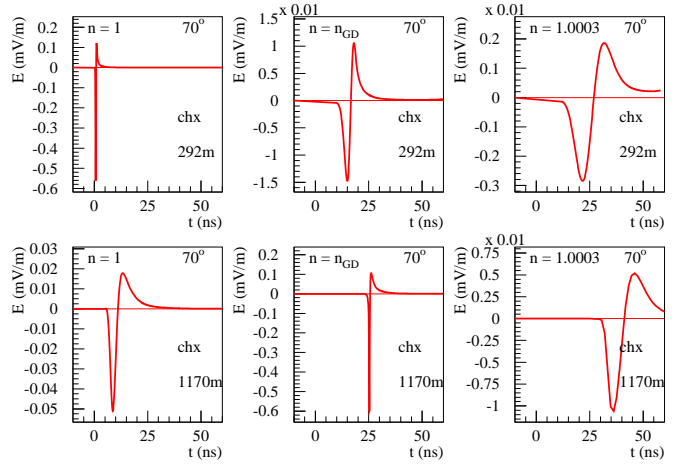


Figure 19: Same as fig 17, but here we consider a more inclined shower.

frequency components occur only at the Cherenkov distance, upon applying a high-pass filter a clear Cherenkov ring should become visible in the LDF. The radius of this ring contains direct information of the shower maximum and thus the chemical composition of the original cosmic ray. New experiments at the Pierre Auger observatory [5, 6], and LOFAR [23] should be able to measure the LDF in more detail, where first hints of “Cherenkov-like” effects might have been observed [4, 22].

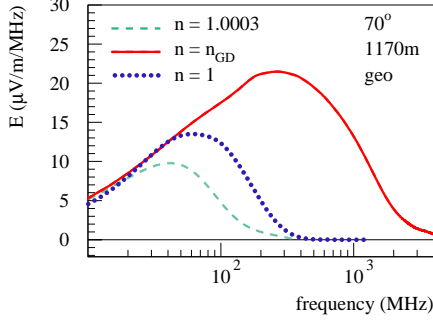


Figure 20: Fourier transform of geomagnetic component of the 70 degrees inclined shower observed at 1170 meters from the shower core. We plot the modulus of the Fourier transform.

V. SUMMARY

We presented a realistic calculation of coherent electromagnetic radiation from air showers initiated by ultra-high energy cosmic rays. The underlying currents are obtained from three-dimensional Monte Carlo simulations of air showers in a realistic geo-magnetic field. We take into account the correct shape of the particle distribution in a shower at a given time. The numerical procedures – simulations, fitting procedures, convolutions, referred to as EVA 1.0 – have been discussed. We showed the importance of a correct treatment of the index of refraction in air, given by the law of Gladstone and Dale: using the correct index of refraction n_{GD} gives very different results compared to a simplified treatment using a constant index, with differences in width and magnitude up to a factor of 100.

Appendix A: Some derivatives

Theorem: The quantity h_k is a function of t and x^\parallel (the transverse coordinates are not considered here). Its derivatives are

$$\frac{d}{dct} h_k = -1, \quad \frac{d}{dx^\parallel} h_k = 1. \quad (\text{A1})$$

The time derivatives of ct^* and $\tilde{R}V$ vanish:

$$\frac{d}{dct} ct^* = \frac{d}{dct} \tilde{R}V = 0. \quad (\text{A2})$$

Proof:

In the following, we do not consider explicitly the transverse coordinates (to be considered constant). The variables of interest are the time $ct \equiv x^0$ and the longitudinal coordinate $x^\parallel \equiv z$. We use for any function $f(t, z)$ the

notation $\partial^0 f = \partial f / \partial ct$, $\partial^z f = -\partial f / \partial z$. For the “total” derivatives, we use $d^0 f = df / dct$, $d^z f = -df / dz$.

We consider for given fixed h the retarded time $t^*(t, z - h)$. The retarded time corresponding to a critical time is given as

$$t_k^* = t^*(t_k, z - h), \quad (\text{A3})$$

with $t_k = t_k(z - h)$. So we have $t_k^* = t_k^*(z - h)$. We have

$$d^z t_k^* = \partial^0 ct^* d^z t_k + \partial^z t^*. \quad (\text{A4})$$

In the following we make extensively use of definitions and relations from reference [16]. For $t = t_k$, we have

$$\tilde{R}V = c(t_k - t_k^*) + \tilde{R}_j V^j|_{t^*=t_k^*} = 0. \quad (\text{A5})$$

We compute the derivative d^z :

$$0 = d^z ct_k - d^z ct_k^* + (\bar{g}_j^z - \tilde{V}_j d^z ct_k^*) V^j \quad (\text{A6})$$

$$= d^z ct_k - (1 - \tilde{V}^j V_j) d^z ct_k^* + \bar{V}^z \quad (\text{A7})$$

$$= d^z ct_k - \tilde{V} V d^z ct_k^* + \bar{V}^z \quad (\text{A8})$$

$$= d^z ct_k - \tilde{V} V (\partial^0 ct^* d^z ct_k + \partial^z ct^*) + \bar{V}^z, \quad (\text{A9})$$

which leads to (using $\bar{V}^z = \bar{V}^\parallel$)

$$d^z ct_k = \frac{-\bar{V}^\parallel + \tilde{V} V \partial^z ct^*}{1 - \tilde{V} V \partial^0 ct^*}. \quad (\text{A10})$$

Using

$$\partial^\alpha ct^* = \frac{\bar{R}^\alpha}{\tilde{R}V}, \quad (\text{A11})$$

we get

$$d^z ct_k = -\frac{\bar{V}^\parallel - \tilde{V} V \bar{R}^\parallel / \tilde{R}V}{1 - \tilde{V} V \bar{R}^0 / \tilde{R}V}. \quad (\text{A12})$$

The time derivative of h_k as obtained from its definition is

$$d^0 h_k = (d^z ct_k)^{-1}, \quad (\text{A13})$$

which gives

$$d^0 h_k = -\frac{\tilde{R}V - \tilde{V} V \bar{R}^0}{\tilde{R}V \bar{V}^\parallel - \tilde{V} V \bar{R}^\parallel}. \quad (\text{A14})$$

Using $\tilde{R}V = 0$, and $\bar{R}^\parallel \approx L = \bar{R}^0$, we find

$$d^0 h_k = -1. \quad (\text{A15})$$

The other derivative of h_k is trivial:

$$d^z h_k = -1. \quad (\text{A16})$$

The potential A , its denominator $\tilde{R}V$, and also the argument ct^* of its numerator J are evaluated at the parallel coordinate $x^\parallel - h_k + \lambda$, so the total time derivatives are

$$d^0 = \partial^0 + d^0 h_k \partial^z, \quad (\text{A17})$$

explicitly

$$d^0 = \partial^0 - \partial^z. \quad (\text{A18})$$

We get

$$d^0 ct^* = (\partial^0 - \partial^z) ct^* = \frac{\bar{R}^0 - \bar{R}^z}{\tilde{R}V} = 0, \quad (\text{A19})$$

and with

$$\partial^\alpha \tilde{R}V = \bar{V}^\alpha - \tilde{V}V \partial^\alpha ct^* \quad (\text{A20})$$

(eq. (22) from [16]), we obtain

$$d^0 \tilde{R}V = 0. \quad (\text{A21})$$

-
- [1] H. Falcke, et al., *Nature* **435**, 313 (2005).
 - [2] W. D. Apel, et al., *Astropart. Physics* **26**, 332 (2006).
 - [3] D. Ardouin, et al., *Astropart. Physics* **26**, 341 (2006).
 - [4] A. Corstanje et al, "LOFAR: Detecting Cosmic Rays with a Radio Telescope", arXiv:1109.5805v1, Contribution to the 32nd International Cosmic Ray Conference (Beijing, China, 11-18 Aug. 2011).
 - [5] J. Coppens et al. (Pierre Auger Collaboration), *Nucl. Instrum. Methods Phys. Res., Sect. A* **604**, S41 (2009).
 - [6] S. Fliescher et al. (Pierre Auger Coll.), Contribution to the 2010 ARENA conference, *Nucl. Instr. and Meth. A* (in print); <http://dx.doi.org/10.1016/j.nima.2010.11.045>.
 - [7] H. R. Allan, *Prog. in Element. part. and Cos. Ray Phys.* **10**, 171 (1971).
 - [8] F.D. Kahn and I.Lerche, *Proc. Royal Soc. London* **A289**, 206 (1966).
 - [9] N.A. Porter, C.D. Long, B. McBreen, D.J.B Murnaghan and T.C. Weekes, *Phys. Lett.* **19**, 415 (1965).
 - [10] J. V. Jelley et al., *Nature* **205**, 327 (1965).
 - [11] O. Scholten, K. Werner, and F. Rusydi, *Astropart. Phys.* **29**, 94 (2008).
 - [12] K.D. de Vries, A.M. van den Berg, O. Scholten, K. Werner, *Astropart. Phys.* **34**, 267 (2010).
 - [13] M. Ludwig and T. Huege, proceedings of ARENA 2010, *Nucl. Instr. and Meth. A* (in print); doi:10.1016/j.nima.2010.10.115 .
 - [14] J. Alvarez-Mu, W.R. Carvalho Jr., E. Zas, arXiv:1107.1189v1
 - [15] T. Huege et al., proceedings of ARENA 2010, *Nucl. Instr. and Meth. A* (in print); doi:10.1016/j.nima.2010.11.041 .
 - [16] K. Werner, O. Scholten, *Astropart. Phys.* **29**: 393-411, 2008, arXiv:0712.2517.
 - [17] K.D. de Vries, A.M. van den Berg, O. Scholten, K. Werner, *Phys.Rev.Lett.* **107**:061101,2011
 - [18] G. Bossard, H.J. Drescher, N.N. Kalmykov, S. Ostapchenko, A.I. Pavlov, T. Pierog, E.A. Vishnevskaya, and K. Werner, *Phys. Rev. D* **63**, 054030, (2001)
 - [19] T. Bergmann R. Engel, D. Heck, N.N. Kalmykov, Sergey Ostapchenko, T. Pierog, T. Thouw, and K. Werner , *Astropart. Phys.* **26**, 420 (2007)
 - [20] K.D. de Vries, O. Scholten, and K. Werner, *Nucl. Instrum. Methods Phys. Res., Sect. A* **662**, S175 (2012)
 - [21] ANITA Collab: S. Hoover et al., To be submitted to *Phys. Rev. Lett* arXiv:1005.0035v2
 - [22] W. D. Apel et al. (LOPES Collaboration), *Astropart. Phys.* **32**, 294 (2010).
 - [23] A. Horneffer et al. (LOFAR CR-KSP Collaboration), *Nucl. Instrum. Methods Phys. Res., Sect. A* **617**, 482 (2010).